Suppression of cavitation inception by gas bubble injection: A numerical study focusing on bubble-bubble interaction

Masato Ida*
Center for Computational Science and E-systems, Japan Atomic Energy Agency, Higashi-Ueno, Taito-ku, Tokyo 110-0015, Japan

Takashi Naoe and Masatoshi Futakawa
J-PARC Center, Japan Atomic Energy Agency, Tokai-mura, Ibaraki-ken 319-1195, Japan
(Received 29 May 2007; published 10 October 2007)

The dynamic behavior of cavitation and gas bubbles under negative pressure has been studied numerically to evaluate the effect of gas bubble injection into a liquid on the suppression of cavitation inception. In our previous studies, it was demonstrated by direct observation that cavitation occurs in liquid mercury when mechanical impacts are imposed, and this will cause cavitation damage in spallation neutron sources, in which liquid mercury is bombarded by a high-power proton beam. In the present paper, we describe numerical investigations of the dynamics of cavitation bubbles in liquid mercury using a multibubble model that takes into account the interaction of a cavitation bubble with preexisting gas bubbles through bubble-radiated pressure waves. The numerical results suggest that, if the mercury includes gas bubbles whose equilibrium radius is much larger than that of the cavitation bubble, the explosive expansion of the cavitation bubble (i.e., cavitation inception) is suppressed by the positive-pressure wave radiated by the injected bubbles, which decreases the magnitude of the negative pressure in the mercury.

DOI: 10.1103/PhysRevE.76.046309 PACS number(s): 47.55.dp, 47.55.dd

I. INTRODUCTION

Cavitation in liquid mercury is now a significant issue in the development of pulsed high-power spallation neutron sources, in which liquid mercury is bombarded by a high-intensity proton beam to produce high neutron fluxes. In off-beam experiments [1,2], it was suggested that high-intensity pressure waves originating from the energy release due to spallation reactions would cause cavitation in liquid mercury, and the associated erosion (i.e., cavitation erosion) would significantly reduce the lifetime of the target vessel in which liquid mercury flows. After this crucial suggestion, research groups in Japan and the United States performed various investigations aimed at overcoming this issue, which concerns the realizability of liquid-mercury spallation targets [3–10].

One of the potential approaches to mitigating the cavitation erosion or preventing the cavitation itself is to inject gas bubbles into liquid mercury. As has been demonstrated in previous studies [11,12], gas bubbles in a liquid change the dynamic and acoustic properties of the liquid and can, in some situations, act as an absorber of sound through their volume change or volume oscillation in response to pressure change. In a recent study, Okita *et al.* showed numerically that the injection of microbubbles into liquid mercury drastically reduces the amplitude of pressure waves if the size and volume fraction of bubbles are suitably controlled, and it would thus effectively suppress cavitation inception [5,6]. In that study, two mechanisms for the reduction of sound amplitude were suggested. One is the absorption of the thermal expansion of liquid mercury caused by the energy release. When spallation reactions occur in liquid mercury, a large amount of thermal energy is released, and then a rapid thermal expansion of liquid mercury and associated increase of pressure take place, which will cause the radiation of high-intensity pressure waves. The injected gas bubbles act as an absorber of the thermal expansion by shrinking themselves. The other suggested mechanism is the attenuation of propagating pressure waves due to bubble oscillation. As has been demonstrated by many authors, the acoustic properties of bubbly liquids depend on the size and volume fraction of the injected bubbles. The numerical results given in Refs. [5,6] showed that gas microbubbles with an appropriate number density can significantly attenuate the pressure wave traveling through the gas-liquid mixture, because of the dispersion effect of the bubbles and the thermal damping of the bubbles' oscillation.

In the present paper, based on some basic experimental data, we have examined numerically the effect of gas bubble injection on the mechanically induced cavitation in liquid mercury and have found one more mechanism responsible for cavitation suppression. In the numerical study, we focus our attention on the acoustic interaction between cavitation bubbles and injected gas bubbles and discuss how the pressure waves radiated by the injected gas bubbles affect the dynamics of cavitation bubbles. The theoretical model used is a Rayleigh-Plesset-type system of equations that takes into account bubble-bubble interactions through the bubble-radiated pressure waves. From the numerical study, we found that the radial motion of the injected bubbles in response to the pressure change decreases the magnitude of the negative pressure in liquid mercury and, consequently, the explosive expansion of small cavitation bubbles is effectively suppressed, because the change in negative pressure enlarges the critical initial radius, which is defined to be the threshold for cavitation inception: for a given negative pressure, bubbles having an initial radius larger than the critical value will

*ida.masato@jaea.go.jp

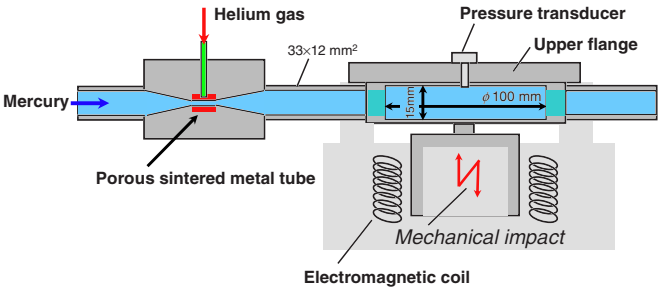

FIG. 1. (Color online) Experimental setup for pressure measurement. The shallow cylinder of 100 mm in diameter and 15 mm in height filled with liquid mercury of about 120 ml is the main body of this experimental system. Mechanical impacts are imposed on the cylinder from the bottom by electromagnetic force. The pressure transducer is replaced with a glass window when the image of bubbles is recorded by high-speed cameras. When examining the effect of gas bubble injection, helium gas is injected into the mercury through a porous sintered metal tube. Pure liquid mercury or a helium-mercury mixture flows into and out from the cylinder through a rectangular channel.

expand explosively, but the others will not. A simple theoretical investigation has also been made of the amplitude of the bubble-radiated pressure waves and their effect on cavitation inception. Our recent experiments have confirmed that gas bubble injection indeed reduces cavitation erosion substantially [13].

The rest of this paper is organized as follows. In Sec. II, the experiment that we performed recently and some basic findings, on which the present numerical study is based, are briefly introduced. The magnitude of the negative pressure appearing in liquid mercury under mechanical impact is the main concern in the experiment. In Sec. III, model equations are presented that describe the radial motion of cavitation and injected gas bubbles interacting with each other through pressure waves. Section IV presents numerical results and discussions of bubble dynamics in experimentally relevant situations and the pressure waves radiated by the injected bubbles, and finally Sec. V summarizes this paper.

II. EXPERIMENT AND BASIC RESULTS

This section introduces our recent experiments, which triggered the present numerical study. Figure 1 illustrates the experimental setup used for measuring pressure in liquid mercury under mechanical impact. This is an off-beam experimental system for impact tests to simulate the cavitation event in real mercury spallation targets, and can well reproduce the morphology of spallation-induced erosion damage [2]. A shallow cylinder of 100 mm diameter and 15 mm height, made of stainless steel, is filled with about 120 ml of liquid mercury (not degassed), on which mechanical impacts are imposed from the bottom using an electromagnetic coil. The characteristics of the output of the electromagnetic coil (pressure amplitude, wave form, etc.) are controlled by the input electric current. The pressure change in the mercury is measured by a pressure transducer (Entran, EPXH) placed on the lower surface of the upper flange of the cylinder. The

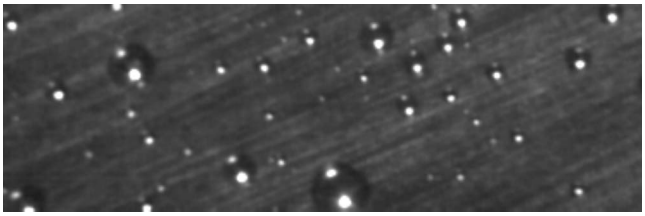

FIG. 2. Helium bubbles in liquid mercury observed through a glass window placed on the surface of the mercury. The height of this image corresponds to 1.62 mm.

images of the bubbles are monitored by high-speed cameras [a high-speed shutter camera (NAC, DiCAM PRO) and a high-speed video camera (NAC, Memrecam fx RX6)] by replacing the upper flange with a clear glass window which enables us to observe the bubbles in liquid mercury (being an opaque liquid), in contact with the window; see Refs. [2,9,10] for greater details of the experimental setup for pressure measurement and image capturing.

Helium gas is injected using a porous sintered metal tube (tungsten), through which gas microbubbles are produced. The flow rate of the injected gas is 6.8 ml/min, which is 0.1% that of the mercury. The helium-mercury mixture flows into and out from the shallow cylinder through a rectangular channel whose cross-sectional area is 33×12 mm^2. Since liquid mercury is an opaque liquid, we do not know the exact condition of the gas bubbles produced in the bulk of the mercury. In the present experimental setup, only the bubbles touching the glass window are observable; the average radius of the observed gas bubbles and the average distance between neighboring bubbles deduced from images taken through the glass window are about 100 and 500 μm, respectively; see Fig. 2.

Typical pressure changes generated by a single mechanical impact with (the solid line) and without (the dashed line) using the bubble injection are shown in Fig. 3. In the present study, compressive impacts of an input power of 560 W were imposed on the mercury, producing a positive-pressure pulse

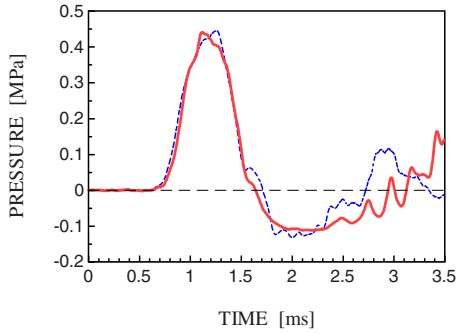

FIG. 3. (Color online) Typical pressure changes (low-pass filtered) in the mercury generated by a single mechanical impact. The solid red and the dashed blue lines, respectively, denote the pressure changes with and without bubble injection. It is seen that the magnitude of the negative pressure was decreased by the bubble injection, implying that the tensile stress in the mercury was reduced by the injected bubbles.

followed by a negative-pressure region. As shown in our previous papers, which reported the direct observation of cavitation bubbles in liquid mercury [9,10], the negative pressure in the case of no bubble injection triggers cavitation, which will cause serious erosion damage when a large number of mechanical impacts are applied [2].

The pressure-time curves in the two cases are qualitatively the same as each other, but their maximum magnitudes in the negative-pressure phase are slightly, but clearly, different; the magnitude was decreased by the gas bubble injection. As another interesting observation, in the case with bubble injection, cavitation bubbles were never found and only injected bubbles undergoing volume change were recorded by the high-speed cameras. These experimental findings suggest that the injected bubbles suppressed cavitation inception, and the difference found between the two measured pressures has a significant influence on the dynamics of cavitation bubbles. In Sec. IV, by computing the dynamic behavior of bubbles under negative pressure, we discuss how the injected gas bubbles alter the negative-pressure value and cavitation bubble dynamics. The theoretical model used in the numerical study is introduced in the next section.

III. MODEL EQUATIONS

The dynamics of bubbles is studied using a nonlinear model based on the Keller-Miksis equation, a variant of the Rayleigh-Plesset equation, which describes the radial motion of a spherical bubble in a compressible liquid:

$$\left(1-\frac{\dot{R}}{c}\right)R\ddot{R}+\left(\frac{3}{2}-\frac{\dot{R}}{2c}\right)\dot{R}^2=\frac{1}{\rho}\left(1+\frac{\dot{R}}{c}\right)p_s+\frac{R}{\rho c}\frac{d}{dt}p_s, \tag{1}$$

$$p_s=p_b-\frac{2\sigma}{R}-\frac{4\mu\dot{R}}{R}-p_{dr}(t)-P_0, \tag{2}$$

where $R=R(t)$ is the time-dependent radius of the bubble, $c=1450$ m/s is the sound speed of liquid mercury, $\rho=13\,528$ kg/m^3 is its density, p_b is the pressure inside the bubble, $\sigma=0.47$ N/m is the surface tension, $\mu=1.52\times10^{-3}$ Pa s is the viscosity of liquid mercury, $p_{dr}(t)$ is the driving pressure acting on the bubble, $P_0=0.1013$ MPa is the atmospheric pressure, and the overdots denote the time derivative d/dt. Equation (1) governs the temporal evolution of the bubble radius and Eq. (2) represents the difference between the pressure in the liquid at the bubble surface and that far away from the bubble.

In multibubble cases, if the center-to-center distances between bubbles are small enough, the pressures acting on the bubbles are not equal to the external driving pressure because the amplitude of the pressure waves radiated by the neighboring bubbles is no longer negligible. Thus, one must take bubble-bubble interaction into consideration, which is known to change the dynamic properties of bubbles in a variety of ways (see Refs. [14–20] for recent studies on bubble-bubble interaction through bubble-radiated pressure waves). The multibubble model used in the present study is derived as follows. The amplitude of the pressure wave radiated by a spherical bubble undergoing volume change can be obtained from the Euler and continuity equations of fluid flow,

$$\frac{\partial u}{\partial t}+u\frac{\partial u}{\partial r}=-\frac{1}{\rho}\frac{\partial p}{\partial r}, \tag{3}$$

$$\frac{\partial r^2u}{\partial r}=0, \tag{4}$$

where $u(r,t)$ and $p(r,t)$ are the velocity and the pressure, respectively, in the liquid phase and r is the radial axis corresponding to the distance from the center of the bubble. Integrating Eq. (4) along the radial axis yields

$$u=\frac{R^2}{r^2}\dot{R}, \tag{5}$$

where we used $u(R,t)=\dot{R}(t)$ and assumed $u(r\to\infty,t)=0$. Substituting Eq. (5) into Eq. (3) and integrating it, one obtains

$$p=\frac{\rho}{r}\frac{d(R^2\dot{R})}{dt}+O\left(\frac{1}{r^4}\right), \tag{6}$$

where we assumed $p(r\to\infty,t)=0$. Hereafter, the bubbles and their physical parameters are identified by numerical subscripts $1,2,\ldots,N$, where N is the total number of bubbles, and the ith bubble is called bubble i. Replacing $p_{dr}(t)$ in Eq. (2) with

$$p_{ex}(t)+\sum_{j=1,j\neq i}^{N}p_j, \tag{7}$$

where $p_{ex}(t)$ is the external driving pressure originating from the mechanical impact, and neglecting high-order terms as suggested in Ref. [14] (see Appendix A of the present paper for details), a modified equation for bubble i is given as follows:

$$\left(1-\frac{\dot{R}_i}{c}\right)R_i\ddot{R}_i+\left(\frac{3}{2}-\frac{\dot{R}_i}{2c}\right)\dot{R}_i^2=\frac{1}{\rho}\left(1+\frac{\dot{R}_i}{c}\right)p_{s,i}+\frac{R_i}{\rho c}\frac{d}{dt}p_{s,i}-\sum_{j=1,j\neq i}^{N}\frac{1}{D_{ij}}\frac{d(R_j^2\dot{R}_j)}{dt}, \tag{8}$$

$$p_{s,i}=p_{b,i}-\frac{2\sigma}{R_i}-\frac{4\mu\dot{R}_i}{R_i}-p_{ex}(t)-P_0, \tag{9}$$

where D_{ij} is the distance between the centers of bubbles i and j. The last term of Eq. (8) describes the acoustic interaction between the bubbles and couples the equations of bubbles $1-N$. The time-delay effect due to the finite sound speed of the surrounding liquid (see, e.g., Ref. [19]) is not considered here because c times a typical duration time of the negative pressure (~0.5 ms), being about 1 m, is much larger than D_{ij} considered below, which is a few millimeters.

The pressure inside the bubbles, $p_{b,i}$, is assumed to obey a van der Waals type of equation (see, e.g., Refs. [21,22]),

$$p_{b,i} = \left(P_0 + \frac{2\sigma}{R_{i0}}\right)\left(\frac{R_{i0}^3 - h_i^3}{R_i^3 - h_i^3}\right)^{\kappa_i}, \tag{10}$$

where R_{i0} is the equilibrium radius of bubble i at atmospheric pressure, for which the bubble's internal pressure balances the liquid pressure through the pressure jump due to the surface tension, and h_i is the hard-core radius ($=R_{i0}/11.26$ for mercury and $R_{i0}/9.81$ for helium) of bubble i, which represents the volume excluded by the total volume of gas molecules as hard spheres, and is considerable when the gas is strongly compressed. The vapor pressure of mercury, 0.28 Pa, is neglected because it is much smaller than P_0 and the absolute value of the negative pressure considered below. The polytropic exponent κ_i of the gas inside bubble i, which reflects the effect of thermal conduction, is roughly determined as $\kappa_i=1$ for $R_i(t) > \beta R_{i0}$ with $\beta \approx 0.2$ and $\kappa_i = \gamma$ otherwise, where γ is the specific heat ratio of the gas (5/3 for mercury and helium). As is known, violently collapsing bubbles behave adiabatically during a very short time when they become very small and their surface velocity $|\dot{R}|$ is very high (see, e.g., Refs. [21–23]). The present setting of κ_i is a rough approximation of this known behavior. This determination of κ_i is rather crude but is sufficient for the present study, because the expansion phase of bubbles in negative pressure is our main concern. More detailed and accurate modeling of bubble dynamics in liquid mercury will be presented in the future.

Despite their simple form, the model equations used in the present study, Eqs. (8) and (9), can be considered to exhibit a high accuracy in a wide range of parameters. Using a simpler, but essentially similar, model, Bremond *et al.* [20] have demonstrated recently that, even when the maximum radii of expanding bubbles reach nearly 75% of half of the interbubble distance and the bubbles are slightly deformed due to the nonuniformity of the pressure around the bubbles' surfaces, this kind of model can provide an accurate result during the first expansion and subsequent collapse.

IV. NUMERICAL INVESTIGATIONS

Let us study bubble dynamics in experimentally relevant situations by numerically solving the multibubble model. We mainly focus our attention on how the pressure waves radiated by injected bubbles affect the dynamics of cavitation bubbles. In this investigation we reduce the problem to a few-bubble problem, and attempt to clarify the basic mechanism of cavitation suppression by bubble injection. Also, the external driving pressure p_{ex} is idealized as

$$p_{ex} = \begin{cases} -1.25P_0 & \text{for } 0 \text{ s} < t \le t_d, \\ -1.25(2 - t/t_d)P_0 & \text{for } t_d < t \le 2t_d, \\ 0P_0 & \text{otherwise}, \end{cases} \tag{11}$$

where $-1.25P_0$ is a typical experimental value of negative pressure and $t_d \sim 0.5$ ms is its duration time; see Fig. 4(b). We should note here that the positive wave front found in Fig. 3 is neglected in this setting since it does not alter bubble dynamics in the negative-pressure period. In Fig. 5, we show numerical results for the dynamics of single bubbles (a small mercury bubble of $R_{i0}=10$ μm and a large helium bubble of $R_{i0}=100$ μm) given using Eqs. (1) and (2). In this computation, we used two kinds of driving pressure: one was the pressure change obtained experimentally without the bubble injection (the dashed blue line in Fig. 3) and the other was its clipped version derived by setting the pressure change to zero when it is positive; see Fig. 5(c). As depicted by the thin red curves in Figs. 5(a) and 5(b), when the nonclipped pressure change was used as the driving pressure, both bubbles shrunk mildly in the first positive-pressure period and then expanded explosively in the subsequent negative-pressure period. The behavior of the bubbles in the negative-pressure period was not notably changed by using the clipped pressure change, as depicted by the thick blue curves in the same figures. This numerical result confirms that the positive wave front has, at least in the pressure change observed in our off-beam experiment, no significant influence on bubble dynamics in the negative-pressure period and hence is negligible in our study. (In a recent study, Bremond *et al.* reached a similar conclusion through experimental and numerical investigations of cavitation in water [20].)

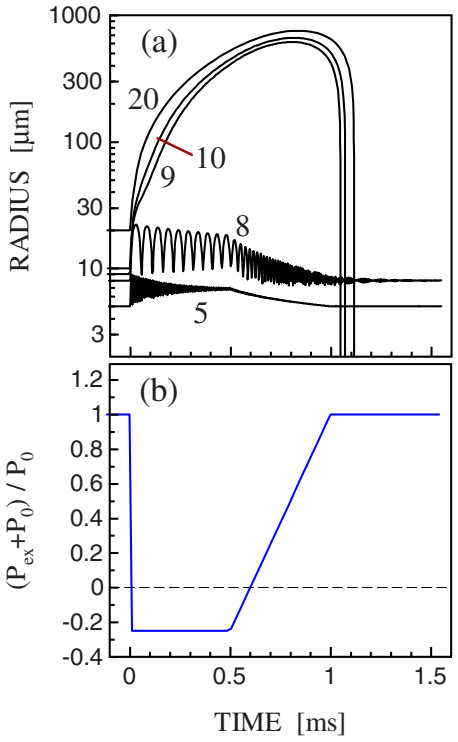

FIG. 4. (Color online) (a) Radius-time curves for single bubbles of $R_{i0}=5$, 8, 9, 10, and 20 μm (from bottom to top), and (b) pressure in the mercury assumed in the numerical study, normalized by P_0. The numbers shown in (a) denote the initial radii (μm) of the bubbles.

First we consider a single-bubble problem ($D_{ij} \to \infty$) to determine the dynamic critical initial radius R_{dc} for the negative pressure defined above. Figure 4(a) shows the dynamics of single cavitation bubbles for different equilibrium radii with $t_d=0.5$ ms. This result means that R_{dc} is in the range of 8–9 μm, because the bubbles of $R_{i0} \ge 9$ μm expanded ex-

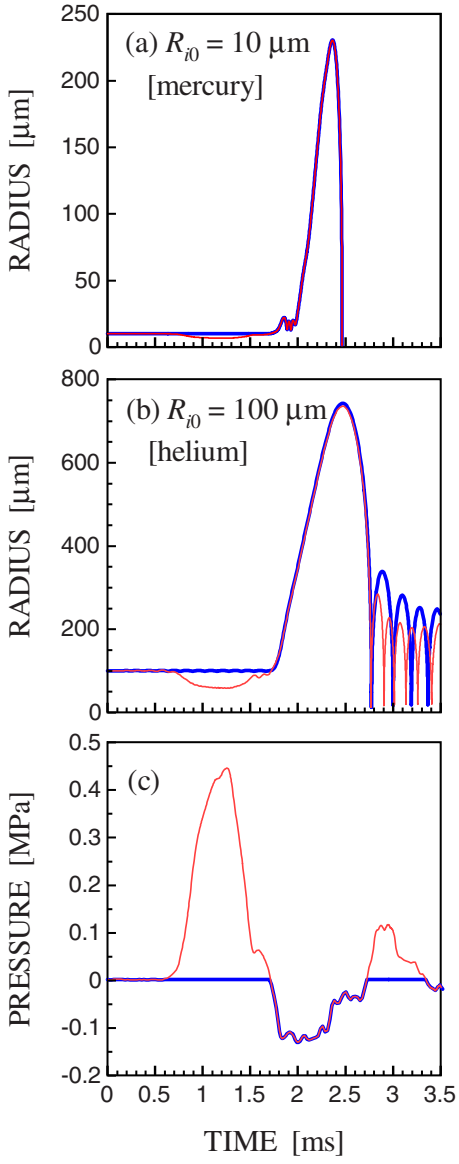

FIG. 5. (Color online) Computed dynamics of (a) a single small mercury bubble of $R_{i0}=10$ μm and (b) a single large helium bubble of $R_{i0}=100$ μm driven by the pressure change given experimentally without bubble injection [the thin red curve in (c)] and its clipped version [the thick blue curve in (c)]. In the negative-pressure period, no notable difference can be found between the results for the original and the clipped pressure changes [the thin red curves and the thick blue curves, respectively, in (a) and (b)].

plosively (implying the occurrence of cavitation inception) but the others exhibited a small-amplitude oscillation. Since we are interested in explosively expanding bubbles, in the following we consider only bubbles larger than the critical size.

Next we consider a two-body problem ($N=2$), that is, the interaction of a cavitation bubble (bubble 1) and an injected gas bubble (bubble 2). Examples of the dynamics of two coupled bubbles for $R_{10}=10$ μm and $R_{20}=100$ μm with different D_{12} are shown in Fig. 6. Here, we assumed that the injected gas bubble has an initial radius much larger than that of the cavitation bubble, as in the experiment, and t_d

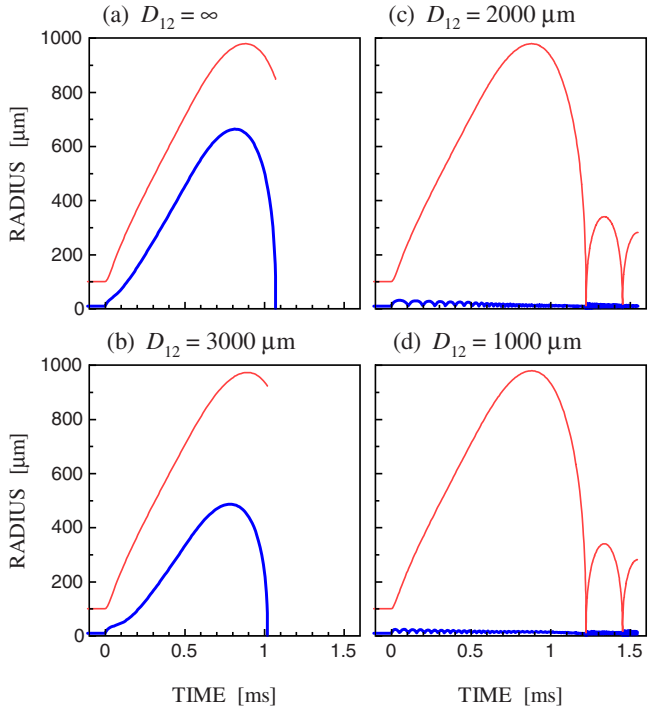

FIG. 6. (Color online) Radius-time curves of a double-bubble system for $R_{10}=10$ μm and $R_{20}=100$ μm with four different D_{12} as indicated in the panels. The thick blue curves and the thin red curves are for the cavitation and the gas bubble, respectively. It should be noted that the computation was stopped when the cavitation bubble violently collapsed. The explosive expansion of the cavitation bubble observed for $D_{12}\geq 3000$ μm is suppressed by the neighboring large gas bubble when $D_{12}\leq 2000$ μm.

$=0.5$ ms, as in the single-bubble study. Interestingly, when $D_{12}\leq 2000$ μm, the explosive expansion of bubble 1 observed for $D_{12}\geq 3000$ μm is completely suppressed by the neighboring gas bubble. Results for different pairs of bubbles with $D_{12}=2000$ μm are shown in Fig. 7. The gas bubble of $R_{20}=100$ μm, which could suppress cavitation inception when $R_{10}=10$ μm [Figs. 6(c) and 6(d)], cannot suppress it when $R_{10}\geq 15$ μm. However, if the gas bubble has a larger radius ($R_{20}=300$ μm; see the right column of Fig. 7) it can achieve cavitation suppression even for $R_{10}=15$ μm. These numerical results indicate that, if the physical parameters are appropriately set, a single gas bubble can have a significant impact on the dynamics of nearby cavitation bubbles and can thus suppress cavitation inception.

We have performed a parametric study to provide greater details of the dependence of the cavitation suppression on the bubble radii and interbubble distance. Figures 8 and 9 show the expansion ratios of the bubbles, $\max(R_i)/R_{i0}$, for different R_{10} and D_{12} as functions of R_{20}. From them, we know that a sufficiently large gas bubble with a sufficiently small D_{12} can completely suppress the explosive expansion of the cavitation bubble and a larger gas bubble or smaller D_{12} is needed for a larger cavitation bubble to suppress its expansion. In the following we discuss the physical mechanism underlying these observations.

It is evident that, in the above numerical examples, the bubble-bubble interaction through the bubble-radiated pres-

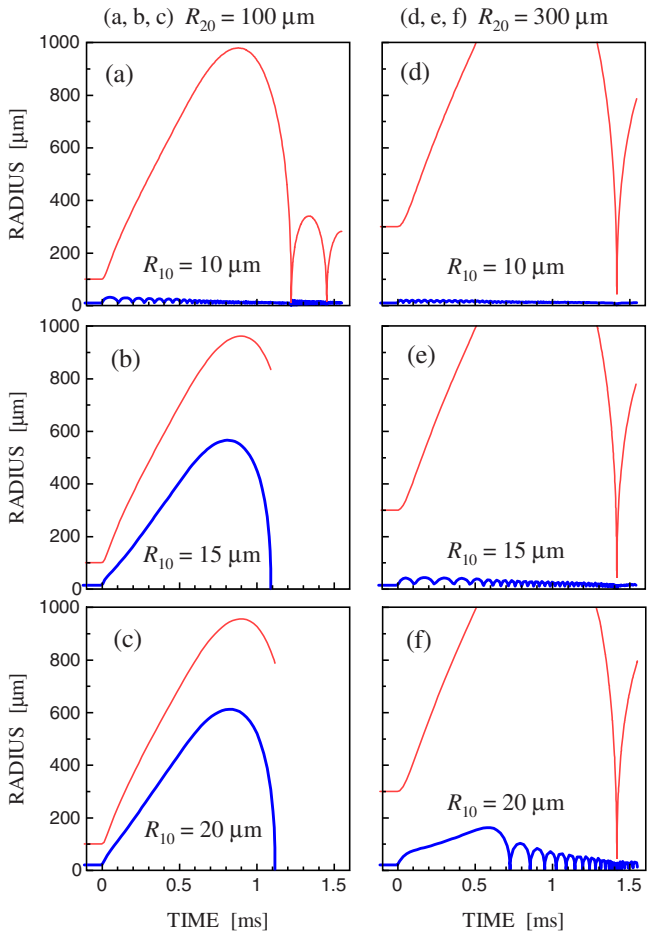

FIG. 7. (Color online) Radius-time curves of six different couples of bubbles for D_{12}=2000 μm. The thick blue curves and the thin red curves are for the cavitation and the gas bubble, respectively. The left and right columns are for R_{20}=100 and 300 μm, respectively. This result suggests that a larger gas bubble is needed to suppress the expansion of a larger cavitation bubble.

sure waves is the only factor that caused the cavitation suppression. We thus examine here the pressure wave radiated by the injected bubble, bubble 2. When the explosive expansion of bubble 1 is suppressed, bubble 2 can act as a single bubble because the amplitude of the pressure wave from bubble 1 is very small. As is known, the expansion velocity of a single bubble expanding explosively under a constant negative pressure (p_{ng}) can be estimated by a simple theoretical formula [24],

$$\dot{R} = \sqrt{\frac{-2p_{ng}}{3\rho}}, \tag{12}$$

where, in our case,

$$p_{ng} = P_0 - 1.25P_0 = -0.25P_0$$

and the vapor pressure was neglected as before. Equation (12) is derived from the Rayleigh-Plesset or the Keller-Miksis equation by assuming that the terms proportional to $1/R^n$ $(n \geq 1)$ are negligible and $\ddot{R} \approx 0$ (see Appendix B for details). This formula says that the expansion velocity in steady growth does not depend on the equilibrium radius R_0 and hence, in general, $R_i(t) > R_j(t)$ if $R_{i0} > R_{j0}$, meaning that a bubble of a larger R_0 is always larger than a bubble of a smaller R_0. Using Eqs. (6) and (12) and assuming $\ddot{R}_2 \approx 0$, we obtain the amplitude of the pressure wave radiated by bubble 2, p_2, measured at the position of bubble 1,

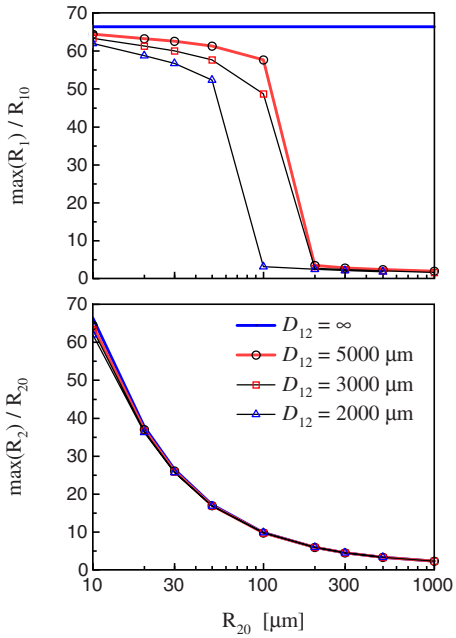

FIG. 8. (Color online) Expansion ratios of bubbles for R_{10} = 10 μm and different D_{12} as functions of R_{20}. It should be noted that the results in cases where $R_1 + R_2 > D_{12}$ was observed during the computation are not shown in this figure.

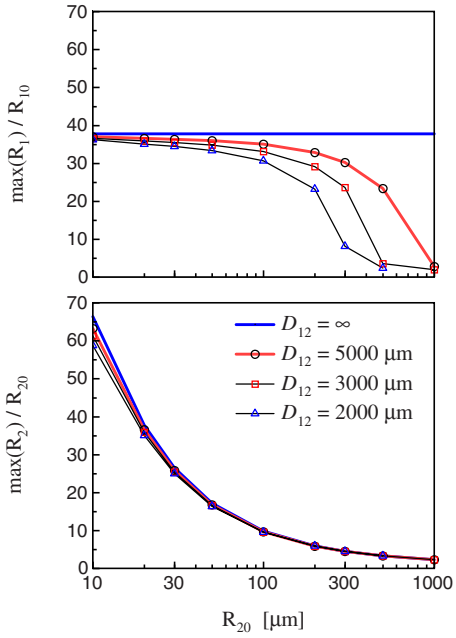

FIG. 9. (Color online) Same as Fig. 8, but for R_{10}=20 μm.

$$p_2(t) \approx -\frac{4}{3}\frac{R_2(t)}{D_{12}}p_{ng}. \tag{13}$$

The total pressure acting on bubble 1, $p_{t,1}$, for $p_{ex}=-1.25P_0$ is thus

$$p_{t,1} = p_{ng} + p_2 \approx -0.25P_0 + \frac{1}{3}\frac{R_2}{D_{12}}P_0. \tag{14}$$

Equation (13) says that p_2 is proportional to R_2 but inversely proportional to D_{12}, which confirms the previous numerical result suggesting that a large injected bubble with a small D_{12} can have a strong impact on cavitation bubble dynamics. More importantly, Eq. (13) proves that p_2 is positive and hence decreases the magnitude of the negative pressure acting on bubble 1. Figure 10(b) shows the total pressure acting on bubble 1 in the case of $R_{10}=10$ μm and $R_{20}=100$ μm with $D_{12}=2000$ μm (the solid curve) and ∞ (the dash-dotted curve) [the former corresponding to the case in Fig. 7(a)], determined numerically using $P_0+p_{ex}+(\rho/D_{12})d(R_2^2\dot{R}_2)/dt$ [i.e., using Eq. (6)]. This clearly shows that the pressure wave radiated by bubble 2 increases the pressure and thus reduces the tensile stress acting on bubble 1. The same figure also shows $p_{t,1}$ for $D_{12}=2000$ μm given by Eq. (14) with R_2 determined numerically. It is in good agreement with the full numerical simulation, confirming the validity of Eq. (13). From this discussion, we can conclude that the cavitation suppression observed in the numerical simulation was induced by the positive pressure radiated by the injected bubble, which decreases the magnitude of the negative pressure acting on the cavitation bubble and hence enlarges the corresponding critical radius. This is consistent with the experimental result shown in Fig. 3.

Lastly, we briefly consider a five-body problem to confirm that a larger number of injected gas bubbles have a stronger impact on cavitation bubble dynamics. In the experiment, a large number of gas bubbles exist in liquid mercury and they interact not only with cavitation bubbles but also with each other, likely resulting in different dynamics from that in double-bubble cases. Hence, it is meaningful to consider a case of more than one gas bubble and compare the results with those in the case of only one gas bubble. Here, we examine the interaction of a cavitation bubble (bubble 1) with four identical gas bubbles (bubbles 2–5) arranged symmetrically around the cavitation bubble; see Fig. 11. Due to the symmetry, the dynamics of bubbles 2–5 will be completely the same (i.e., $R_2=R_3=R_4=R_5$), and hence this problem can be reduced to a two-body problem of bubbles 1 and 2 as follows:

$$\left(1-\frac{\dot{R}_1}{c}\right)R_1\ddot{R}_1 + \left(\frac{3}{2}-\frac{\dot{R}_1}{2c}\right)\dot{R}_1^2 = \frac{1}{\rho}\left(1+\frac{\dot{R}_1}{c}\right)p_{s,1} + \frac{R_1}{\rho c}\frac{d}{dt}p_{s,1} - \frac{4}{D_{12}}\frac{d(R_2^2\dot{R}_2)}{dt}, \tag{15}$$

$$\left(1-\frac{\dot{R}_2}{c}\right)R_2\ddot{R}_2 + \left(\frac{3}{2}-\frac{\dot{R}_2}{2c}\right)\dot{R}_2^2 = \frac{1}{\rho}\left(1+\frac{\dot{R}_2}{c}\right)p_{s,2} + \frac{R_2}{\rho c}\frac{d}{dt}p_{s,2} - \frac{1}{D_{12}}\frac{d(R_1^2\dot{R}_1)}{dt} - \left(\frac{1}{2}+\frac{2}{\sqrt{2}}\right)\frac{1}{D_{12}}\frac{d(R_2^2\dot{R}_2)}{dt}. \tag{16}$$

The $\max(R_i)/R_{i0}$ versus R_{20} curves for $R_{10}=20$ μm with different D_{12} are shown in Fig. 12. This result clearly shows that, in this situation, compared to the double-bubble case (Fig. 9), cavitation suppression occurs over a wider range (about three times) of parameter space. The large expansion of bubble 1 in the case of $R_{20}=100$ μm and $D_{12}=2000$ μm observed when $N=2$, for example, is now completely suppressed by the four surrounding bubbles.

An exception is found for $R_{20}=500$ μm with $D_{12}=2000$ μm, a delayed expansion of the cavitation bubble in the period where the four surrounding bubbles are rapidly shrinking. As indicated in Fig. 13, this is due to the negative-pressure waves radiated by the injected bubbles when they have a large negative acceleration. This is an interesting observation and should be examined in more detail, but the accuracy of this case is rather questionable because $2\max(R_2)/\sqrt{2}D_{12}=0.996$ ($\sqrt{2}D_{12}$ being the center-to-center distance between the nearest-neighbor gas bubbles; see Fig. 11) and a more refined model is thus needed to address it; hence we do not discuss it further here.

V. CONCLUSION

We have studied numerically the effect of gas bubble injection on the mechanically induced cavitation in liquid mercury, and have found a mechanism responsible for cavitation suppression: the injected gas bubbles decrease the magnitude of the negative pressure in liquid mercury by radiating a positive-pressure wave in its early stage of expansion, which results in the suppression of the explosive expansion of cavitation bubbles near the injected bubbles. A simple theoretical study has also been performed on the bubble-radiated pressure waves, and confirmed the accuracy and validity of the numerical result. In the future, we must consider a many-bubble system to determine a sufficient number density or volume fraction of injected bubbles, although the present numerical study discussed only few-bubble systems.

A possible concern about the gas bubble injection is whether the injected bubbles also cause erosion. Now we anticipate that the erosion intensity of large gas bubbles is much smaller than that of cavitation bubbles. Figures 8 and 9 show that the expansion ratio of a large bubble is smaller than that of a smaller bubble. This observation suggests that

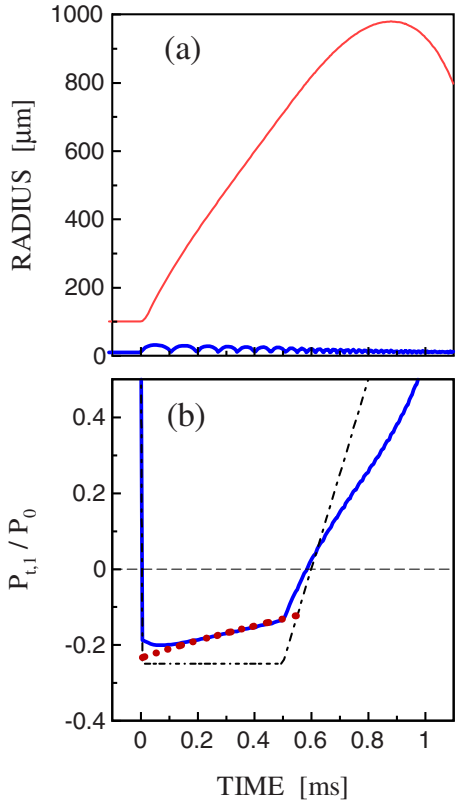

FIG. 10. (Color online) (a) Radius-time curves of bubbles in the expansion phase and (b) total pressure acting on bubble 1 (i.e., the cavitation bubble) for $R_{10}=10$ μm and $R_{20}=100$ μm with $D_{12}=2000$ μm (solid curve) and ∞ (dash-dotted curve). In (a), the thick blue curve and the thin red curve are for the cavitation and the gas bubble, respectively. In (b), the dotted line denotes the total pressure for $D_{12}=2000$ μm obtained theoretically using the simple formula (14). It is clearly shown that the magnitude of the negative pressure is decreased by the positive pressure wave radiated by bubble 2.

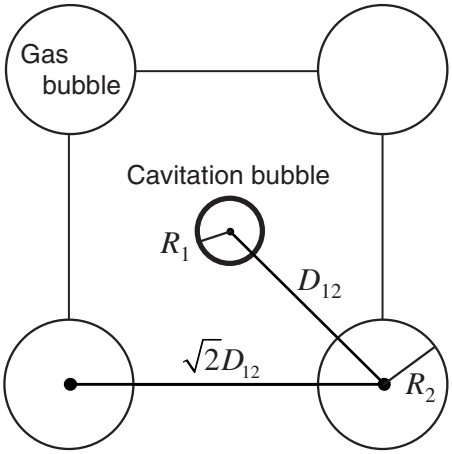

FIG. 11. Five-body problem with a cavitation bubble surrounded by four gas bubbles. Four identical gas bubbles, bubbles 2–5, are arranged symmetrically around a small cavitation bubble, bubble 1, and all the bubbles are located in the same plane. The center-to-center distance between the nearest-neighbor gas bubbles is thus $\sqrt{2}D_{12}$.

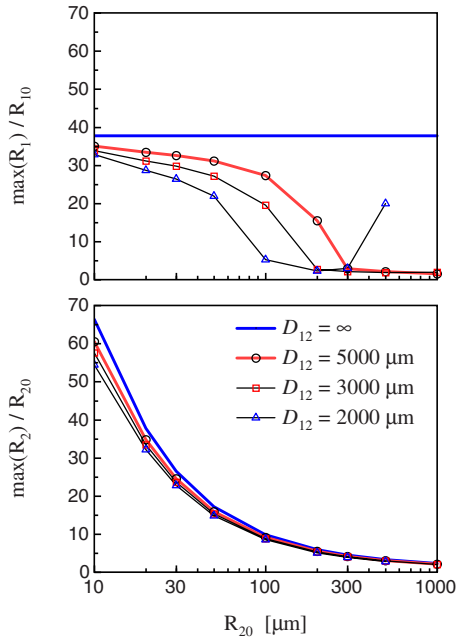

FIG. 12. (Color online) Expansion ratios of bubbles in five-body cases for $R_{10}=20$ μm and different D_{12} as functions of R_{20}.

the collapse velocity of large gas bubbles is smaller than that of small bubbles (similarly to the fact that a strongly stretched spring will have a larger contraction velocity than a

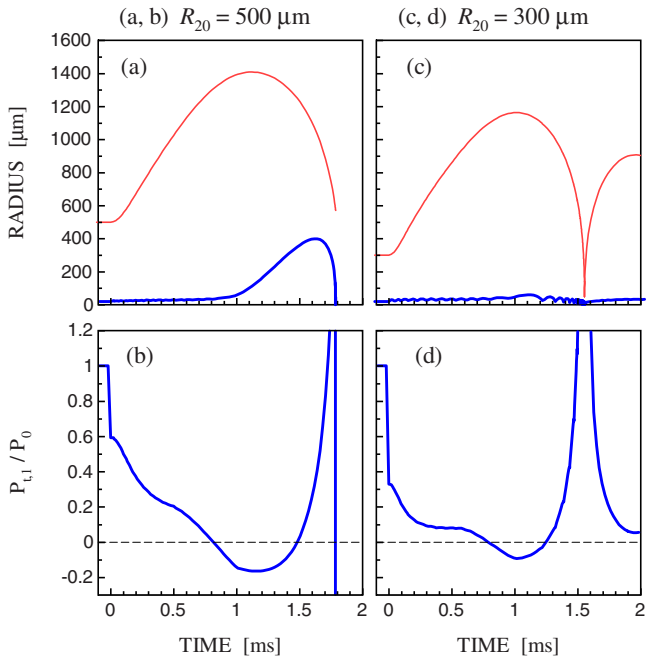

FIG. 13. (Color online) (a) Delayed expansion of cavitation bubble observed for $R_{20}=500$ μm with $D_{12}=2000$ μm and (b) total pressure acting on the cavitation bubble. In (a) [and (c)], the thick blue curve and the thin red curve are for the cavitation and the gas bubble, respectively. The negative pressure appearing when the gas bubbles have a negative acceleration caused the delayed expansion. Such behavior is not found when R_{20} is smaller; see (c) and (d) for $R_{20}=300$ μm.

mildly stretched one). We have also observed in our computation that the maximum collapse velocity of large gas bubbles is much smaller than that of cavitation bubbles. These observations imply that the erosion intensity of bubbles having a large equilibrium radius (i.e., in our case, injected gas bubbles) is much smaller than that of bubbles having a quite small equilibrium radius (i.e., cavitation bubbles). Lastly, we stress again that our recent experiments have confirmed that the gas bubble injection that we have attempted can indeed reduce cavitation erosion substantially even in cases where a large number of mechanical impacts are imposed on the liquid mercury [13,25]. The details of the experimental results and also more extensive numerical and theoretical investigations will be presented elsewhere.

ACKNOWLEDGMENTS

This work was partly supported by the Ministry of Education, Culture, Sports, Science, and Technology of Japan through a Grant-in-Aid for Young Scientists (B) (No. 17760151) and by the Japan Society for the Promotion of Science through Grants-in-Aid for Scientific Research (No. 17360085 and No. 17560740).

APPENDIX A: TRUNCATED TERMS IN THE COUPLED KELLER-MIKSIS EQUATION

Upon substitution of Eq. (7) into Eqs. (1) and (2), the following terms, other than those involved in Eq. (8), are derived from Eq. (1):

$$-\sum_{j=1,j\neq i}^{N}\left(\frac{\dot{R}_i}{c}\frac{1}{D_{ij}}\frac{d(R_j^2\dot{R}_j)}{dt}+\frac{R_i}{c}\frac{1}{D_{ij}}\frac{d^2(R_j^2\dot{R}_j)}{dt^2}\right). \quad \text{(A1)}$$

The terms in large parentheses can be rewritten as

$$\frac{R_j}{D_{ij}}\frac{\dot{R}_i}{c}(2\dot{R}_j^2+R_j\ddot{R}_j)+\frac{R_i}{D_{ij}}\frac{\dot{R}_j}{c}(2\dot{R}_j^2+6R_j\ddot{R}_j)+R_j^2\frac{R_i}{D_{ij}}\frac{d^2}{dt^2}\left(\frac{\dot{R}_j}{c}\right). \quad \text{(A2)}$$

From this, one knows that the terms in Eq. (A1) are of order $(R_j/D_{ij})(\dot{R}_i/c)$ or $(R_i/D_{ij})[d^2(\dot{R}_j/c)/dt^2]$ and thus negligible in Eq. (8).

APPENDIX B: DERIVATION OF THE EXPANSION VELOCITY UNDER CONSTANT NEGATIVE PRESSURE

Assuming that $|\dot{R}|\ll c$, $dp_{dr}/dt=0$, and $R(t)$ is large enough so that the terms in Eq. (2) proportional to $1/R^n$ $(n\geq 1)$ are negligible compared to $p_{dr}+P_0$, Eq. (1) is reduced to

$$R\ddot{R}+\frac{3}{2}\dot{R}^2=-\frac{p_{dr}+P_0}{\rho}. \quad \text{(B1)}$$

Assuming $\ddot{R}\approx 0$ and rearranging yields

$$\dot{R}=\sqrt{\frac{-2(p_{dr}+P_0)}{3\rho}}. \quad \text{(B2)}$$

Upon substitution of $p_{dr}+P_0=p_{ng}$ into this, one obtains Eq. (12).

The expansion velocity in our cases is on the order of 1 m/s and is much smaller than c (1450 m/s). The assumption of $|\dot{R}|\ll c$ used in deriving the above formula is thus fully satisfied.

[1] M. Futakawa, H. Kogawa, R. Hino, H. Date, and H. Takeishi, Int. J. Impact Eng. **28**, 123 (2003).
[2] M. Futakawa, T. Naoe, H. Kogawa, C.-C. Tsai, and Y. Ikeda, J. Nucl. Sci. Technol. **40**, 895 (2003).
[3] M. Futakawa, T. Naoe, C. C. Tsai, H. Kogawa, S. Ishikura, Y. Ikeda, H. Soyama, and H. Date, J. Nucl. Mater. **343**, 70 (2005).
[4] J. R. Haines, B. W. Riemer, D. K. Felde, J. D. Hunn, S. J. Pawel, and C. C. Tsai, J. Nucl. Mater. **343**, 58 (2005).
[5] K. Okita, Y. Matsumoto, and S. Takagi, in Proceedings of FEDSM2005, ASME Fluids Engineering Division Summer Meeting and Exhibition, Houston, Texas (2005), p. 1–6.
[6] K. Okita, A. Fujiwara, S. Takagi, Y. Matsumoto, and M. Futakawa, in Proceedings of the Sixth International Symposium on Cavitation, CAV2006, Wageningen, The Netherlands (2006), p. 1-10.
[7] A. Fujiwara, K. Okita, Y. Matsumoto, M. Futakawa, S. Hasegawa, H. Kogawa, and Y. Ikeda, in Proceedings of the 17th Meeting of the International Collaboration on Advanced Neutron Sources (ICANS-XVII), Santa Fe, New Mexico (Los Alamos National Laboratory, LA-UR 06–3904, 2006), Vol. II, p. 552.
[8] K. Thomsen, J. Nucl. Mater. **356**, 321 (2006).
[9] T. Naoe, M. Futakawa, T. Koyama, and H. Kogawa, Jikken Rikigaku **6**, 301 (2006) (in Japanese).
[10] M. Ida, T. Naoe, and M. Futakawa, Phys. Rev. E **75**, 046304 (2007).
[11] E. L. Carstensen and L. L. Foldy, J. Acoust. Soc. Am. **19**, 481 (1947); Z. Ye and A. Alvarez, Phys. Rev. Lett. **80**, 3503 (1998); M. Kafesaki, R. S. Penciu, and E. N. Economou, *ibid.* **84**, 6050 (2000).
[12] L. V. Wijngaarden, Annu. Rev. Fluid Mech. **4**, 369 (1972); K. W. Commander and A. Prosperetti, J. Acoust. Soc. Am. **85**, 732 (1989); M. Kameda and Y. Matsumoto, Phys. Fluids **8**, 322 (1996).
[13] M. Futakawa, H. Kogawa, S. Hasegawa, M. Ida, K. Haga, T. Wakui, T. Naoe, N. Tanaka, Y. Matsumoto, and Y. Ikeda, in Proceedings of the 18th Meeting of the International Collaboration on Advanced Neutron Sources (ICANS-XVIII), Dongguan, Guangdong Province, China, 2007 (unpublished).
[14] R. Mettin, I. Akhatov, U. Parlitz, C. D. Ohl, and W. Lauterborn, Phys. Rev. E **56**, 2924 (1997).

[15] M. Ida, Phys. Lett. A **297**, 210 (2002); M. Ida, J. Phys. Soc. Jpn. **71**, 1214 (2002).
[16] A. Ooi and R. Manasseh, ANZIAM J. **46**(E), C102, (2005).
[17] M. Ida, Phys. Rev. E **72**, 036306 (2005).
[18] M. Ida, Phys. Fluids **17**, 097107 (2005).
[19] A. A. Doinikov, R. Manasseh, and A. Ooi, J. Acoust. Soc. Am. **117**, 47 (2005).
[20] N. Bremond, M. Arora, S. M. Dammer, and D. Lohse, Phys. Fluids **18**, 121505 (2006).
[21] S. Hilgenfeldt, S. Grossmann, and D. Lohse, Phys. Fluids **11**, 1318 (1999).
[22] M. P. Brenner, S. Hilgenfeldt, and D. Lohse, Rev. Mod. Phys. **74**, 425 (2002).
[23] K. Yasui, Phys. Rev. E **56**, 6750 (1997).
[24] C. E. Brennen, *Cavitation and Bubble Dynamics* (Oxford University Press, New York, 1995).
[25] T. Naoe, M. Ida, and M. Futakawa (unpublished).